# Mixing state of oxalic acid containing particles in the rural area of Pearl River Delta, China: implications for the formation mechanism of oxalic acid

Chunlei Cheng[1,2], Mei Li[1,2*], Chak K. Chan[3], Haijie Tong[4], Changhong Chen[5], Duohong Chen[6], Dui Wu[1,2], Lei Li[1,2], Cheng Wu[1,2], Peng Cheng[1,2], Wei Gao[1,2], Zhengxu Huang[1,2], Xue Li[1,2], Zhijuan Zhang[1,2], Zhong Fu[7], Yanru Bi[7], Zhen Zhou[1,2*]

[1]Institute of Mass Spectrometer and Atmospheric Environment, Jinan University, Guangzhou 510632, China
[2]Guangdong Provincial Engineering Research Center for on-line source apportionment system of air pollution, Guangzhou 510632, China
[3]School of Energy and Environment, City University of Hong Kong, Hong Kong, China
[4]Max Planck Institute for Chemistry, Multiphase Chemistry Department, Hahn-Meitner-Weg 1, 55128 Mainz, Germany
[5]State of Environmental Protection Key Laboratory of the formation and prevention of urban air pollution complex, Shanghai Academy of Environmental Sciences, Shanghai 200233, China
[6] State Environmental Protection Key Laboratory of Regional Air Quality Monitoring, Guangdong Environmental Monitoring Center, Guangzhou, 510308, China
[7]Guangzhou Hexin Analytical Instrument Limited Company, Guangzhou 510530, China

*Correspondence to*: Mei Li (limei2007@163.com) and Zhen Zhou (zhouzhen@gig.ac.cn)
Tel: 86-20-85225991, Fax: 86-20-85225991

**Abstract**:

The formation of oxalic acid and its mixing state in atmospheric particulate matter (PM) were studied using a single particle aerosol mass spectrometer (SPAMS) in the summer and winter of 2014 in Heshan, a supersite in the rural area of the Pearl River Delta (PRD) region in China. Oxalic acid-containing particles accounted for 2.5% and 2.7% in total detected ambient particles in summer and winter, respectively. Oxalic acid was measured in particles classified as elemental carbon (EC), organic carbon (OC), elemental and organic carbon (ECOC), biomass burning (BB), heavy metal (HM), secondary (Sec), sodium-potassium (NaK) and dust. Oxalic acid was found predominantly mixing with sulfate and nitrate during the whole sampling period, likely due to aqueous phase reactions. In summer, oxalic acid-containing particle number and ozone concentration followed a very similar trend, which may reflect the significant contribution of photochemical reactions to oxalic acid formation. The favorable in-situ pH (2-4) and the dominance of transition metal ions in oxalic acid particles can be plausibly explained by the enhanced production of •OH from Fenton like reaction, which can promote the oxalic acid production from the oxidation of precursors by •OH in HM type particles. In wintertime, carbonaceous type particles contained a substantial amount of oxalic acid as well as abundant carbon clusters and biomass burning markers. The general existence of nitric acid and high relative acidity ratio in oxalic acid-containing particles indicates an acidic environment during the formation process of oxalic acid. The peak areas of nitrate, sulfate and oxalic had similar temporal change in the carbonaceous type oxalic acid particles, and the organosulfate-containing oxalic acid particles well correlated with total oxalic acid particles during the episode, which suggests the formation of oxalic acid is closely associated with acid-catalyzed reactions of organic precursors.

**Keywords**: Oxalic acid; Single particles; Mixing state; Photochemical process; Aqueous phase reactions.

## 1. Introduction

Organic aerosol, typically a large fraction of fine particles, contains more than thousands of organic compounds and contributes to visibility reduction, photochemical smog, climate change and adverse health effects (Novakov and Penner, 1993;Goldstein and Galbally, 2007;Jimenez et al., 2009;Poschl and Shiraiwa, 2015). A significant component of organic aerosol is secondary organic aerosol (SOA) formed from the gas phase oxidation of volatile organic compounds (VOCs) followed by partitioning of products into particles or from heterogeneous reactions of VOCs with particles (Hallquist et al., 2009;Zhang et al., 2015). Dicarboxylic acids (DCAs) are abundant and ubiquitous constituents in SOA and can be effective tracers for the oxidative processes leading to the formation of SOA (Kawamura and Ikushima, 1993;Ervens et al., 2011;Wang et al., 2012;Cheng et al., 2013). DCAs normally have high water solubility and low vapor pressure, so they play important roles in controlling the hygroscopic properties of organic aerosols (Prenni et al., 2003;Ma et al., 2013) and activating cloud condensation nuclei (Booth et al., 2009). The primary emissions of DCAs from anthropogenic sources in urban areas are minor (Huang and Yu, 2007;Stone et al., 2010), and they are mainly derived from secondary oxidation of VOCs and subsequent intermediates (Ho et al., 2010;Myriokefalitakis et al., 2011). High concentrations of DCAs have been observed in biomass burning plume (Kundu et al., 2010;Kawamura et al., 2013) with more than 70% of DCAs produced from photochemical oxidation of water-soluble organic compounds, and only a small contribution from direct biomass burning emission (van Pinxteren et al., 2014).

The production of DCAs through photochemical reactions has been reported in many field studies via the analysis of the diurnal and seasonal variations of DCA(Kawamura and Ikushima, 1993;Kawamura and Yasui, 2005;Aggarwal and Kawamura, 2008;Pavuluri et al., 2010;Ho et al., 2011;Wang et al., 2017), but the mechanism of DCAs formation is still not well understood. Oxalic acid is usually the most abundant DCA observed in the field (Kawamura et al., 2004;Ho et al., 2007;Kawamura et al., 2010). A number of ground based and airborne field studies

have found a tight correlation between oxalic acid and sulfate in ambient particles and cloud droplets, relating aqueous phase chemistry to the formation of oxalic acid in aerosols and cloud droplets (Yao et al., 2002;Yao et al., 2003;Yu et al., 2005;Sorooshian et al., 2006;Sorooshian et al., 2007a;Sorooshian et al., 2007b;Miyazaki et al., 2009;Wonaschuetz et al., 2012;Wang et al., 2016). In recent years, several model and laboratory studies suggested that the aqueous phase oxidation of highly water-soluble organics like glyoxal, methylglyoxal and glyoxylic acid can efficiently produce oxalic acid in aerosol particles and cloud droplets (Lim et al., 2010;Myriokefalitakis et al., 2011;Ervens et al., 2014;Yu et al., 2014;McNeill, 2015). Recent stable carbon isotope studies and field observations have also suggested that oxalic acid forms through aqueous phase reactions (Wang et al., 2012;Cheng et al., 2015). However, the detailed formation mechanisms of oxalic acid from photochemistry and aqueous phase chemistry in ambient aerosols are still not comprehensively understood and need to be further studied.

Online measurements of the size distribution of oxalic acid-containing particles and the mixing state of oxalic acid with other compounds in aerosols are useful to examine the formation and evolution of oxalic acid and SOA particles. Sullivan and Prather investigated the diurnal cycle and mixing state of DCA-containing particles in Asian aerosol outflow using aerosol time-of-flight mass spectrometry (ATOFMS), and proposed the formation of DCA on Asian dust (Sullivan and Prather, 2007b). In addition, Yang et al. (2009) measured oxalic acid particles in Shanghai and proposed that in-cloud processes and heterogeneous reactions on hydrated aerosols contributed to the formation of oxalic acid (Yang et al., 2009). While the formation mechanism of oxalic acid especially in urban areas is still not clear, online measurements of the mixing state of oxalic acid provide a powerful tool to better understand the formation of oxalic acid in aerosol particles and cloud droplets.

The Pearl River Delta (PRD) region has distinct meteorological seasonality under the influence of the Asian monsoon system, which brings air from the ocean in spring and summer, and carries polluted air from northern China in autumn and winter. Strong photochemical activity occurs in summer under the condition of high

temperature and relative humidity, and in winter high loadings of particles from northern cities are favorable for the occurrence of haze episode (Bi et al., 2011;Zhang et al., 2013;Zhang et al., 2014). Here we present the seasonal field measurements of the mixing state of oxalic acid-containing particles using a single particle aerosol mass spectrometer (SPAMS) in a rural supersite of the PRD region. The seasonal characteristic of oxalic acid particles and mixing state with secondary species were investigated to explore the formation mechanisms of oxalic acid and aging process of SOA.

# 2. Methods

## 2.1 Aerosol sampling

Particles were sampled using a single particle aerosol mass spectrometer (SPAMS) at the Guangdong Atmospheric Supersite (22.73N, 112.93E), a rural site at Heshan city (Figure S1). The supersite is surrounded by farm land and villages, with no local industrial or traffic emissions. Ambient aerosols were sampled to the SPAMS through a 2.5m long copper tube with 0.5m of the sampling inlet located above the top of the building. The measurement period was from July 18 to August 1 in 2014, and from January 27 to February 8 in 2015. Real-time $PM_{2.5}$ mass concentration was simultaneously measured by a TEOM monitor (series 1405, Thermo scientific), and hourly concentrations of $O_3$ were measured by an $O_3$ analyzer (model 49i, Thermo scientific). The local meteorological data including temperature, relative humidity and visibility were measured on the rooftop of the building. The average temperature during the field study was 29.5℃ in summer and 14.1℃ in winter and the average relative humidity was 71.7% and 63% in summer and winter, respectively.

## 2.2 SPAMS

Real-time measurements of single atmospheric particles has been demonstrated by Prather and co-workers in the 1990s using aerosol time-of-flight mass spectrometry (ATOFMS) (Prather et al., 1994;Noble and Prather, 1996). Based on the same principle, the single particle aerosol mass spectrometer (SPAMS) developed by Guangzhou Hexin Analytical Company was applied to field measurements of single

particles in the current work. The details of the SPAMS system have been introduced previously (Li et al., 2011). Briefly, aerosol particles are sampled into the vacuum pumped aerodynamic lens of the SPAMS through an electro-spark machined 80μm critical orifice at a flow rate of 75 ml $min^{-1}$. The individual particles with a terminal velocity are introduced to the sizing region. The velocity of each single particle is detected by two continuous laser beams (diode Nd:YAG, 532 nm) with a space of 6 cm. The velocity is then used to calculate the single particle aerodynamic diameter and provide the precise timing of the firing of a 266 nm laser used to induce desorption and ionization (Nd:YAG laser, 266nm). The energy of the desorption/ionization 266 nm laser was 0.6 mJ and the power density was kept at about $1.6\times10^{8}$ $W/cm^{2}$ during both sampling periods. The 266 nm laser generates positive and negative ions that are detected by a Z-shaped bipolar time of flight mass spectrometer. The size range of the detected single particles is 0.2 to 2 μm. Polystyrene latex spheres (Nanosphere size standards, Duke Scientific Corp., Palo Alto) of 0.22-2.0 μm diameter were used for size calibration.

**2.3 Data analysis**

The size and chemical composition of single particles detected by SPAMS were analyzed using the COCO toolkit based on the Matlab software. Particles were clustered into several groups using the neural network algorithm (ART-2a) to group particles into clusters with similar mass spectrum features. The ART-2a parameters used in this work were set to a vigilance factor of 0.8, a learning rate of 0.05, and a maximum of 20 iterations. We collected 516,679 and 767,986 particles with both positive and negative mass spectra in summer and winter respectively. A standard solution of oxalic acid was prepared with pure oxalic acid ($H_2C_2O_4$, purity: 99.99%, Aladdin Industrial Corporation) and atomized to aerosols. After drying through two silica gel diffusion driers, pure oxalic acid particles were directly introduced into the SPAMS. The positive and negative mass spectra of oxalic acid are shown in Figure S2. Based on the mass spectra of pure oxalic acid and previous ambient measurements by ATOFMS (Silva and Prather, 2000;Sullivan and Prather, 2007b;Yang et al., 2009), $HC_2O_4^-$ (m/z -89) is selected as the ion peak for oxalic acid containing particles. In

this work, oxalic acid particles are identified if the peak area of m/z -89 was larger than 0.5% of the total signal in the mass spectrum. With this threshold, 13109 and 20504 of oxalic acid-containing particles were obtained in summer and winter separately, accounting for 2.5% and 2.7% of the total detected particles. The percentage of oxalic acid-containing particles in total particles in this work was comparable to the reported value in the urban area of Shanghai (3.4%) (Yang et al., 2009). However, these percentages are in general much lower than those reported in cleaner environments such as the western Pacific Ocean where oxalic acid was found in up to 1-40% of total particles due to little anthropogenic influences (Sullivan and Prather, 2007b).

The oxalic acid containing particles are classified into eight types in the following order: elemental carbon (EC), organic carbon (OC), elemental and organic carbon (ECOC), biomass burning (BB), heavy metal (HM), secondary (Sec), sodium-potassium (NaK) and dust. Different type particles are identified according to characteristic ion markers and dominant chemical species (Table S1): (1) particles containing abundant carbon clusters like $\pm12[C]^{+/-}$, $\pm24[C_2]^{+/-}$, $\pm36[C_3]^{+/-}$ with relative peak area more than 0.5% are classified as EC type, (2) any remaining particles containing abundant signals of $27[C_2H_3]^+$, $43[C_2H_3O]^+$ and hydrocarbon clusters with relative peak area more than 0.5% are classified as OC type, (3) any remaining particles containing signals of $\pm12[C]^{+/-}$, $\pm24[C_2]^{+/-}$, $37[C_3H]^+$ and $43[C_2H_3O]^+$ with relative peak area more than 0.5% are classified as ECOC type, (4) any remaining particles containing abundant signals of $39[K]^+$ (peak area>1500) with relative peak area of $-59[C_2H_3O_2]^-$ and $-73[C_3H_5O_2]^-$ simultaneously more than 0.5% are classified as BB type, (5) any remaining particles containing signals of $55[Mn]^+$, $56[Fe]^+$, $63/65[Cu]^+$, $64[Zn]^+$ and $208[Pb]^+$ with relative peak area more than 0.5% are classified as HM type, (6) any remaining particles containing abundant signals of $18[NH_4]^+$ (peak area>50), $-62[NO_3]^-$ (peak area>100) and $-97[HSO_4]^-$ (peak area>100) are classified as Sec type, (7) any remaining particles containing abundant signals of $23[Na]^+$ (peak area>1500) and related species are classified as NaK type, (8) any remaining particles containing signals of $40[Ca]^+$, $56[CaO]^+$ and related species are

classified as dust type. The rules for oxalic acid particles classification in the current work have been reported in previous studies (Sullivan and Prather, 2007a;Yang et al., 2009;Zhang et al., 2013;Li et al., 2014).

### 2.4 Inorganic ions and in-situ pH ($pH_{is}$)

Water-soluble inorganic ions and trace gases were determined by an online analyzer for monitoring aerosols and gases (MARGA, model ADI 2080, Applikon Analytical B. V. Corp., the Netherlands) with a $PM_{2.5}$ sampling inlet at one hour resolution from July 18 to August 1 in 2014. The principle and instrumental design has been described in detail elsewhere (ten Brink et al., 2007;Du et al., 2011;Behera et al., 2013;Khezri et al., 2013). Standard solutions containing all detected ions were injected into MARGA before and after the field measurement. The liquid water content and the concentration of $H^+$ in particles are calculated using the ISORROPIA II model (Nenes et al., 1998, 1999;Fountoukis and Nenes, 2007). We choose stable mode and reverse type in the ISORROPIA model to calculate the concentration of $H^+$ and the liquid water content in this work. The in-situ pH ($pH_{is}$) of particles is calculated through the following equation:

$$pH_{is} = -\log\alpha_{H^+} = -\log(\gamma_{H^+} \times n_{H^+} \times 1000/V_a) \quad (1)$$

where $n_{H^+}$ is the concentration of $H^+$ (mol $m^{-3}$) and $V_a$ is the volume concentration of the $H_2O$ ($cm^3$ $m^{-3}$) , while $\gamma_{H^+}$ is the activity coefficient of $H^+$(Xue et al., 2011;Cheng et al., 2015). The temporal variation of $pH_{is}$ of ambient $PM_{2.5}$ particles is presented in Figure S3, and demonstrated that 97% of particles were acidic in summer.

## 3. Results and Discussion

### 3.1 Seasonal variation of oxalic acid containing particles

The clustered 48 hr back trajectories of air masses arriving in Heshan during the sampling period are shown in Figure S4. In summer, air masses at 500m levels above the ground were mainly from the ocean and rural areas with less influence of human activity, while in winter air masses were directly from urban areas of Guangzhou and Foshan, indicating a strong influence from anthropogenic emissions. The temporal

variations of the total detected particles and oxalic acid containing particles in summer and winter are shown in Figure 1. The total particles had similar trends with the mass concentration of ambient $PM_{2.5}$, suggesting that the counts of total particles detected by SPAMS can be representative of $PM_{2.5}$ mass concentration during the whole sampling periods. The oxalic acid ($C_2$-containing) particles, in general, exhibited distinct diurnal peaks from July 28 to August 1, while they showed different temporal trends in winter. The relative abundance of oxalic acid particles in all of the sampled particles ($C_2$/total ratio) had the same variation with the abundance of oxalic acid particles in summer, especially in the period of July 28 – August 1 (Figure 1). In winter, however, particle counts and relative abundance of oxalic acid had different temporal changes except Jan 30 and February 5-8, when the count and relative abundance of oxalic acid particles simultaneously had a sudden increase.

The oxalic acid-containing particles were clustered into eight groups, and they altogether accounted for 89.6% and 95.1% of total oxalic acid particles in summer and winter, respectively. Table 1 shows that in summer heavy metal (HM) type particles contributed 31.3% to total oxalic acid particles, followed by the Sec (19.2%) and BB type (13%). However, in winter BB type particles were the most abundant and accounted for 24.2% of the oxalic acid-containing particles, followed by EC and HM type. Besides, carbonaceous type particles including EC, OC, ECOC and BB accounted for 28.1% of oxalic acid particles in summer and 59.8% in winter, indicating the seasonal different characteristics of oxalic acid particles. The temporal variations of eight groups of oxalic acid particles in summer and winter are illustrated in Figure 1. In summer HM type particles (orange color) and total oxalic acid particles exhibited similar diurnal patterns, suggesting a possible connection between the production of oxalic acid and the transition metals (e.g. Fe, Cu) (Zhou et al., 2015). Although Sec, BB and EC type particles showed similar diurnal patterns with total oxalic acid particles, the concentrations of these type particles were generally lower than HM type particles. In winter diurnal variation of oxalic acid particles was not obvious but a sharp increase, accompanied by the increase of BB, EC and Sec type particles, was observed on February 8.

The averaged positive and negative ion mass spectra of oxalic acid containing particles are shown in Figure 2. The positive ion spectrum of oxalic acid particles in summer was characterized by high fractions of metal ion peaks including 23$[Na]^+$, 27$[Al]^+$, 39$[K]^+$, 55$[Mn]^+$, 56$[Fe]^+$, 63/65$[Cu]^+$, 64$[Zn]^+$ and 208$[Pb]^+$, and carbonaceous marker ions at m/z 27$[C_2H_3]^+$, 36$[C_3]^+$, 43$[C_2H_3O/C_3H_7]^+$, 48$[C_4]^+$ (Figure 2 a). The negative ion spectrum of oxalic acid particles in summer was characterized by the strong intensity of secondary ions including m/z -46$[NO_2]^-$, -62$[NO_3]^-$, -79$[PO_3]^-$, -80$[SO_3]^-$, -96$[SO_4]^-$ and -97$[HSO_4]^-$, as well as carbon clusters of -24$[C_2]^-$, -36$[C_3]^-$, -48$[C_4]^-$ and BB markers of -59$[C_2H_3O_2]^-$ and -73$[C_3H_5O_2]^-$ (Figure 2 b) (Zauscher et al., 2013). More carbonaceous clusters, i.e., 27$[C_2H_3]^+$, 29$[C_2H_5]^+$, 36$[C_3]^+$, 37$[C_3H]^+$, 43$[C_2H_3O]^+$, 48$[C_4]^+$, 51$[C_4H_3]^+$, 55$[C_4H_7]^+$, 60$[C_5]^+$, 63$[C_5H_3]^+$, 65$[C_5H_5]^+$, 74$[C_2H_2O_3]^+$, 77$[C_6H_5]^+$, were observed in the positive ion spectrum of oxalic acid particles in winter (Figure 2 c) than in summer. The negative ion spectrum of oxalic acid particles in winter (Figure 2 d) contained a large amount of secondary ions, similar to those found in summer, and a more intense signal of nitric acid (-125$[HNO_3NO_3]^-$) , suggesting an acidic nature of oxalic acid particles in winter.

The mixing state of oxalic acid particles with sulfate, nitrate and ammonium (SNA) was investigated through the percentage of SNA-containing oxalic acid particles in total oxalic acid particles (Figure 3). Oxalic acid was found to be internally mixed with sulfate and nitrate during both sampling periods with percentage of 93% and 94% in summer respectively, and both 98% in winter (Figure 3 a). However, the percentage of $NH_4^+$ with oxalic acid was only 18% in summer but increased to 71% in winter. Linear correlations between $NH_4^+$-containing oxalic acid particles ($C_2$-$NH_4^+$) and total oxalic acid particles are depicted in Figure 3, with better linear regression ($r^2$=0.98) in winter than summer. The low percentage of $NH_4^+$ in oxalic acid particles in summer indicated the presence of oxalic acid in $NH_4^+$-poor particles. Aqueous phase production of $SO_4^{2-}$ has been studied well and the linear correlation between oxalic acid and $SO_4^{2-}$ has been used to study the production of oxalic acid through aqueous phase reactions (Yu et al., 2005;Miyazaki et al.,

2009;Cheng et al., 2015). In our work, oxalic acid and $C_2$-$SO_4^{2-}$ displayed good correlations in summer and winter (both $r^2$=0.99), which suggests a common production route of oxalic acid and sulfate, likely aqueous phase reactions.

Figure 4 shows the unscaled size-resolved number distributions of the eight types of oxalic acid particles. Oxalic acid mainly existed in 0.4 to 1.2 μm particles during the entire sampling period but exhibited different peak modes for each particle type in summer and winter. In summer, major types of oxalic acid particles showed distinct peak mode at different size diameter. EC and Sec type particles peaked at 0.5 μm, followed by BB type particles at 0.55 μm, then HM type particles at 0.6 μm, and OC type particles at 0.7 μm. The difference of peak mode suggests the possible different chemical evolution process for each type oxalic acid-containing particles. However, in winter, oxalic acid particles showed broader size distribution from 0.5 to 0.8 μm for all particle types. Oxalic acid particles of all types were generally larger in winter than summer, possibly due to condensation and coagulation of particles during aging of oxalic acid particles in winter.

**3.2 Photochemical production of oxalic acid in summer**

In summer oxalic acid particles showed peaks in the afternoon especially from July 28 to August 1, which was in agreement with the variation pattern of the $O_3$ concentration (Figure 5), indicating a strong association of oxalic acid formation with photochemical reactions. Malonic acid is another product of photochemical oxidation of organic compounds (Kawamura and Ikushima, 1993;Wang et al., 2012;Meng et al., 2013;Meng et al., 2014). In our campaign, malonic acid containing particles had diurnal trends similar to oxalic acid particles and $O_3$ concentration. As the dominant particle type, HM particles had identical variation pattern with total oxalic acid particles. They are characterized by highly abundant metal ion peaks like 55$[Mn]^+$, 56$[Fe]^+$, 63/65$[Cu]^+$, 64$[Zn]^+$ and 208$[Pb]^+$, as well as secondary ion peaks of -46$[NO_2]^-$, -62$[NO_3]^-$, -80$[SO_3]^-$, -96$[SO_4]^-$ and -97$[HSO_4]^-$ in the negative spectrum in summer (Figure 6). •OH produced from Fenton reactions between $H_2O_2$ and $Fe^{2+/3+}$ in acidic solutions has been considered as a substantial source of •OH(Fenton, 1894;Dunford, 2002;Herrmann et al., 2015). The high abundance of metal ions in

oxalic acid particles may be an indication of possible Fenton reactions in the acidic aqueous phase of acidic particles (pH<5, Figure S3), although we cannot exclude the possibility of gas phase condensation of oxalic onto HM particles.

The oxidation of glyoxal and glyoxylic acid by •OH has been identified as an important pathway of oxalic acid production by field and laboratory studies (Ervens et al., 2004;Ervens and Volkamer, 2010;Wang et al., 2012;Wang et al., 2015). The modeling studies from Ervens et al. (2014) suggest that oxalic acid production from glyoxal and glyoxylic acid in aqueous phase significantly depends on •OH availability (Ervens et al., 2014). The main sources of •OH in the aqueous phase contain both direct uptake from the gas phase and the chemical sources in the aqueous phase such as Fenton type reactions and photolysis of $H_2O_2$, $NO_3^-$, $NO_2^-$, and chromophoric dissolved organic matter (CDOM) (Yu et al., 2014;Badali et al., 2015;Ervens, 2015;Gligorovski et al., 2015;Herrmann et al., 2015;Tong et al., 2016). Considering the low Henry's law constant of •OH ($K_{H,OH}$=30 M $atm^{-1}$) (Hanson et al., 1992) and abundant fraction of transition metal ions in the oxalic acid particles, the photolysis of $H_2O_2$ through Fenton reactions involving the catalysis of transition metal ions like $Fe^{2+/3+}$, $Cu^{+/2+}$ and $Mn^{2+/3+}$ likely contributes substantially to the source of •OH in the aqueous phase in this work (Deguillaume et al., 2005;Herrmann et al., 2005;Ervens et al., 2014). The •OH formation process through Fenton reactions can be expressed as (Ervens, 2015):

$$Fe^{2+} + H_2O_2 \rightarrow FeOH^{2+} + \bullet OH \quad (\text{or } Fe^{3+} + OH^- + \bullet OH) \qquad (R1)$$

$$FeOH^{2+}/Fe^{3+} + HO_2^{\cdot}/O_2^{\cdot-} \rightarrow Fe^{2+} + O_2 + H_2O/OH^- \qquad (R2)$$

The actual chemical process is far more complex and involves iron oxides and iron-complexes, thus in the current work we focus on the potential availability of •OH from Fenton reactions and the impact on the oxidation process of organic precursors.

In order to investigate the photochemical aqueous phase formation of oxalic acid in summer, the diurnal variations of $O_3$, oxalic acid particles, HM group particles and $pH_{is}$ of ambient particles averaged from July 28 to August 1, 2014 are shown in Figure 7. The concentration of $O_3$ increased after 9:00 and peaked at 17:00, while oxalic acid particles and HM group particles both increased after 10:00 and showed

two peaks at 15:00 and 19:00. The prominent photochemical feature of oxalic acid particles suggested a close association of photochemical reactions with oxalic acid production. Although •OH production from Fenton reactions can both occur under dark and light radiation conditions, photo-Fenton reactions may have more contribution to the enhancement of oxalic acid particles in the current work. This was possibly due to the diurnal variation of $pH_{is}$, since Fenton reactions strongly depend on the pH of the aqueous phase (Gligorovski et al., 2015). When pH<1, $Fe^{2+}$ is directly oxidized by $H_2O_2$ to $Fe^{3+}$ with no production of •OH (Barb et al., 1951;Kremer, 2003), and the most favorable pH value for Fenton reaction is between 2.5 and 5 (Deguillaume et al., 2005). In the current work the $pH_{is}$ of ambient particles ranged from -1.42 to 4.01, and the influences of $pH_{is}$ from RH and inorganic ions are discussed in Figure S5. Strongly acidic particles were observed during the whole day with high $pH_{is}$ at 6:00 and after 12:00. Although $pH_{is}$ was around 2 at 6:00, only a few oxalic acid-containing particles were observed during this period due to low abundance of HM particles. Oxalic acid-containing particles were found to increase from 12:00 to 21:00, which was attributed to increased organic precursors from VOCs oxidation and enhanced •OH production from Fenton reactions under $pH_{is}$ at 1-4. The number concentration of oxalic acid particles peaked at 19:00 instead of during the strong photochemical activity period in the afternoon; this was possibly due to the efficient degradation of oxalic acid from the complex with iron (Sorooshian et al., 2013;Zhou et al., 2015). Furthermore, photolysis of $Fe(oxalate)_n^{3-2n}$ can contribute to 99% of the overall degradation of oxalic acid (Weller et al., 2014). Although the enhanced •OH production from photo-Fenton reactions was favorable for the formation of oxalic acid from 12:00 to 18:00, we speculate that a high degradation rate of oxalic acid by iron complexation resulted in a lower net production of oxalic acid than at 19:00. In addition to the contribution from Fenton reactions after 12:00, the precursors of oxalic acid such as glyoxylic acid have higher reaction rate with •OH in high pH solutions due to reported studies(Ervens et al., 2003;Herrmann, 2003;Cheng et al., 2015), thus the increase of pH not only enhances •OH production from photo-Fenton reactions, but also promotes the oxidation process of oxalic acid's

precursors by •OH.

Based on above discussions of the mixing state of oxalic acid with secondary ions and transition metals, a plausible explanation to the formation process of oxalic acid in the HM type oxalic acid particles is proposed (Figure S6). In summer strong photochemical activity and high $O_3$ concentrations in the afternoon lead to more production of reactive radicals such as •OH and $HO_2^{\bullet}$, which promote the oxidation of VOCs to dicarbonyls and aldehydes (e.g. glyoxal and methylglyoxal), followed by a subsequent partitioning into the aqueous phase of particles (Myriokefalitakis et al., 2011). Acidic particles containing transition metals like Fe and Cu potentially yield more •OH in acidic aqueous phase, then hydrated dicarbonyls and aldehydes can be oxidized by •OH to glyoxylic acid and finally to oxalic acid (Wang et al., 2012) (Figure S6). Recently Ma et al. (2015) had studied the Fe-containing particles in the PRD and found Fe-containing particles are more efficient at generating •OH in summer than winter (Ma et al., 2015), which supports the enhanced •OH production in HM type particles in this work. A large amount of Fe related particles are emitted from steel industries in the North China Plain and metals like V, Zn, Cu and Pb from electronic manufacturing (Cui and Zhang, 2008;Dall'Osto et al., 2008). These metals contribute significantly to haze episodes (Moffet et al., 2008;Li et al., 2014), which possibly increases the formation of SOA by yielding more •OH participating the heterogeneous and aqueous reactions.

The diurnal patterns of temperature, wind speed are presented in Figure S7. The high temperature between 9:00 and 19:00 was favorable to the secondary processing of organic precursors. The wind speed was low during the whole day, especially between 9:00 and 18:00, which provided a stagnant environment for the increase in oxalic acid produced from photochemical process. The influence from traffic emission was investigated through the diurnal variations of total EC type particles and $NO_2$ (Figure S7). The EC type particles increased from 12:00 to 21:00, which had same variation as total oxalic acid, but $NO_2$ followed the rush hour pattern with two peaks from 5:00 to 8:00 and from 18:00 to 21:00. Traffic emission is not expected to have a large contribution to oxalic acid in this study.

### 3.3 Formation process of oxalic acid in winter

Despite lower $O_3$ concentrations and photochemical activity in winter, oxalic acid particles were still prevalent in carbonaceous particles, especially BB type particles. While oxalic acid was found to be internally mixed with sulfate and nitrate both in summer and winter, the nitric acid was only observed in oxalic acid particles in winter, indicating a strongly acidic nature of oxalic acid particles in winter. Considering a possible connection of oxalic acid production with the acidic environment, the temporal concentrations of oxalic acid, sulfate and nitrate were investigated through their peak areas in the carbonaceous type oxalic acid particles including EC, OC, ECOC and BB type in Figure 8. The peaks of m/z -62$[NO_3]^-$ and -97$[HSO_4]^-$ represent nitrate and sulfate, respectively. Nitrate, sulfate and oxalic acid showed very similar variation patterns in winter, indicating a close connection of their co-existence. Although nitric acid was found in the oxalic acid particles, the acidity of the oxalic acid particles was not estimated since the real-time concentration of inorganic ions was not available during the sampling period in winter. Instead the relative acidity ratio ($R_{ra}$), defined as the ratio of total peak areas of nitrate and sulfate to the peak area of ammonium (m/z 18$[NH_4]^+$), was used (Denkenberger et al., 2007;Pratt et al., 2009). The $R_{ra}$ of carbonaceous type oxalic acid particles ranged from 7 to 114 with an average value of 25 (Figure 8), indicating an intensely acidic environment of carbonaceous type oxalic acid particles in winter. Several studies have reported potential production of oxalic acid from acid-catalyzed aqueous phase reactions in aerosols (Carlton et al., 2006;Carlton et al., 2007;Tan et al., 2009). In this work the acidic environment of the carbonaceous type oxalic acid particles and similar variation patterns among oxalic acid, sulfate and nitrate may suggest a relationship between the degradation of organic precursors and the acidic chemical process. However, the temporal change of $R_{ra}$ did not follow a similar trend as the peak area of oxalic acid in most particles, possibly due to the multi-step formation of oxalic acid influenced by many factors such as precursors, liquid water content and ion strength (Carlton et al., 2007;Cheng et al., 2013;Cheng et al., 2015).

The sharp increase of oxalic acid particles on February 8, 2015 (Figure 1) was

selected as a typical episode to investigate the formation processes of oxalic acid in winter. During the episode, the 48 hr back trajectory analysis showed air masses that originated from the urban areas of Guangzhou and Foshan city (Figure S4), indicating strong influence on organic precursors from anthropogenic emissions. Oxalic acid particle types were dominated by BB (23.2%), followed by EC (22.0%) and Sec (15.1%) type (Table 2). Carbonaceous particles including EC, ECOC, OC, BB accounted for 61.6% of the total oxalic acid particles. The mass spectra of oxalic acid particles were characterized by many hydrocarbon clusters of 27$[C_2H_3]^+$, 29$[C_2H_5]^+$, 37$[C_3H]^+$, 43$[C_2H_3O]^+$, 51$[C_4H_3]^+$, 55$[C_4H_7]^+$, 63$[C_5H_3]^+$, 65$[C_5H_5]^+$, 74$[C_2H_2O_3]^+$, 77$[C_6H_5]^+$, and carbon clusters of 36$[C_3]^+$, 48$[C_4]^+$, 60$[C_5]^+$ in positive mass spectrum, while the negative mass spectrum was characterized by elemental carbon clusters like -24$[C_2]^-$, -36$[C_3]^-$, -48$[C_4]^-$, biomass burning markers of -59$[C_2H_3O_2]^-$ and -73$[C_3H_5O_2]^-$ and secondary species including -42$[CNO]^-$, -46$[NO_2]^-$, -62$[NO_3]^-$, -79$[PO_3]^-$, -80$[SO_3]^-$, -96$[SO_4]^-$ and -97$[HSO_4]^-$ (Figure 9 a).

As the precursor of oxalic acid, glyoxal has the potential to react with sulfuric acid to produce organosulfates through acid-catalyzed nucleophilic addition according to laboratory and chamber studies(Surratt et al., 2007;Galloway et al., 2009). The negative ion of -155($[C_2H_3O_2SO_4]^-$) has been identified as the marker ion of organosulfates derived from glyoxal in chamber and field measurements using ATOFMS (Surratt et al., 2008;Hatch et al., 2011). The formation of organosulfates from glyoxal requires an acidic aqueous environment, which can be used as an indicator of acid-catalyzed ageing process of organic compounds. The temporal trend of organosulfate-containing oxalic acid particles in winter is shown in Figure S8, which exhibited a similar pattern as the total oxalic acid particles during the whole sampling period in winter. The percentage of organosulfate-containing oxalic acid particles in total oxalic acid particles ranged from 0 to 16.4% with the highest ratio observed in the episode (February 8). The linear regression between total oxalic acid particles and organosulfate-containing oxalic acid particles in the episode is exhibited in Figure 9b, and the robust correlation ($r^2$=0.81) between them suggests that oxalic acid and organosulfate may share similar formation process. Based on the above

discussion, the degradation of carbonaceous species associated with acid-catalyzed reactions may have an important contribution to the formation of oxalic acid during the episode in winter. Similar particle types and mass spectra of oxalic acid-containing particles during the episode and the whole sampling period in winter were observed, which suggest the acid-catalyzed oxidation of organic precursors as a potential source for oxalic acid.

## 4. Summary and conclusions

Oxalic acid containing particles were measured by a single particle aerosol mass spectrometer (SPAMS) in the summer and winter of 2014 in Heshan, China. They accounted for 2.5% and 2.7% of the total detected ambient particles. In summer heavy metal-containing particles were the largest group of particles containing oxalic acid with a fraction of 31.3% followed by Sec type (19.2%), while in winter BB type was the dominant group with a percentage of 24.2%. More than 90% of oxalic acid particles were internally mixed with sulfate and nitrate during the whole sampling period. Only 18% of oxalic acid particles contained ammonium in summer, which increased to 71% in winter. In summer oxalic acid and $O_3$ concentration exhibited similar diurnal variations, indicating a substantial contribution of photochemical reactions to oxalic acid formation. Furthermore, suitable in-situ pH is favorable for Fenton like reactions to produce •OH in HM type particles, and might promote the oxalic acid production from the oxidation of precursors by •OH in HM type particles. In winter carbonaceous type particles including EC, OC, ECOC and BB groups accounted for 59.8% of oxalic acid particles and increased to 61.6% in the episode. Nitric acid and organosulfate were found to co-exist in oxalic acid-containing particles in the winter, which suggests a close association with acid-catalyzed reactions. Acid-catalyzed oxidation of organic precursors is a potential contribution for the formation of oxalic acid in winter. The current study demonstrates that SPAMS is a unique tool for understanding the mixing states of different components of ambient aerosols, which are useful for exploring the formation and evolution process of SOA.

## Acknowledgements

This work was financially supported by National Key Technology R&D Program (Grant No. 2014BAC21B01), Guangdong Province Public Interest Research and Capacity Building Special Fund (Grant No. 2014B020216005), the Strategic Priority Research Program (B) of the Chinese Academy of Sciences (Grant No. XDB05040502), Guangdong Industry-University Research Program (Grant No.2012B090500014), and NSFC of Guangdong Province (Grant No. 2015A030313339). Chak K. Chan would like to acknowledge funding support of the General Fund of National Natural Science Foundation of China (Grant No. 41675117). Haijie Tong acknowledge Max Planck Society for funding and Ulrich Pöschl for helpful discussions.

## References

Aggarwal, S. G., and Kawamura, K.: Molecular distributions and stable carbon isotopic compositions of dicarboxylic acids and related compounds in aerosols from Sapporo, Japan: Implications for photochemical aging during long-range atmospheric transport, Journal of Geophysical Research-Atmospheres, 113, D14301, 10.1029/2007jd009365, 2008.

Badali, K. M., Zhou, S., Aljawhary, D., Antinolo, M., Chen, W. J., Lok, A., Mungall, E., Wong, J. P. S., Zhao, R., and Abbatt, J. P. D.: Formation of hydroxyl radicals from photolysis of secondary organic aerosol material, Atmospheric Chemistry and Physics, 15, 7831-7840, 10.5194/acp-15-7831-2015, 2015.

Barb, W., Baxendale, J., George, P., and Hargrave, K.: Reactions of ferrous and ferric ions with hydrogen peroxide. Part I.—The ferrous ion reaction, Transactions of the Faraday Society, 47, 462-500, 1951.

Behera, S. N., Betha, R., Liu, P., and Balasubramanian, R.: A study of diurnal variations of PM 2.5 acidity and related chemical species using a new thermodynamic equilibrium model, Science of the Total Environment, 452, 286-295, 2013.

Bi, X., Zhang, G., Li, L., Wang, X., Li, M., Sheng, G., Fu, J., and Zhou, Z.: Mixing state of biomass burning particles by single particle aerosol mass spectrometer in the urban area of PRD, China, Atmospheric Environment, 45, 3447-3453, 2011.

Booth, A. M., Topping, D. O., McFiggans, G., and Percival, C. J.: Surface tension of mixed inorganic and dicarboxylic acid aqueous solutions at 298.15 K and their importance for cloud activation predictions, Phys Chem Chem Phys, 11, 8021-8028, 10.1039/b906849j, 2009.

Carlton, A. G., Turpin, B. J., Lim, H. J., Altieri, K. E., and Seitzinger, S.: Link between isoprene and secondary organic aerosol (SOA): Pyruvic acid oxidation

yields low volatility organic acids in clouds, Geophysical Research Letters, 33, L06822, 10.1029/2005gl025374, 2006.
Carlton, A. G., Turpin, B. J., Altieri, K. E., Seitzinger, S., Reff, A., Lim, H. J., and Ervens, B.: Atmospheric oxalic acid and SOA production from glyoxal: Results of aqueous photooxidation experiments, Atmospheric Environment, 41, 7588-7602, 10.1016/j.atmosenv.2007.05.035, 2007.
Cheng, C., Wang, G., Meng, J., Wang, Q., Cao, J., Li, J., and Wang, J.: Size-resolved airborne particulate oxalic and related secondary organic aerosol species in the urban atmosphere of Chengdu, China, Atmospheric Research, 161, 134-142, 2015.
Cheng, C. L., Wang, G. H., Zhou, B. H., Meng, J. J., Li, J. J., Cao, J. J., and Xiao, S.: Comparison of dicarboxylic acids and related compounds in aerosol samples collected in Xi'an, China during haze and clean periods, Atmospheric Environment, 81, 443-449, 10.1016/j.atmosenv.2013.09.013, 2013.
Cui, J. R., and Zhang, L. F.: Metallurgical recovery of metals from electronic waste: A review, J Hazard Mater, 158, 228-256, 10.1016/j.jhazmat.2008.02.001, 2008.
Dall'Osto, M., Booth, M., Smith, W., Fisher, R., and Harrison, R. M.: A study of the size distributions and the chemical characterization of airborne particles in the vicinity of a large integrated steelworks, Aerosol Science and Technology, 42, 981-991, 2008.
Deguillaume, L., Leriche, M., Desboeufs, K., Mailhot, G., George, C., and Chaumerliac, N.: Transition metals in atmospheric liquid phases: Sources, reactivity, and sensitive parameters, Chem Rev, 105, 3388-3431, 10.1021/cr040649c, 2005.
Denkenberger, K. A., Moffet, R. C., Holecek, J. C., Rebotier, T. P., and Prather, K. A.: Real-time, single-particle measurements of oligomers in aged ambient aerosol particles, Environmental Science & Technology, 41, 5439-5446, 10.1021/es070329l, 2007.
Du, H., Kong, L., Cheng, T., Chen, J., Du, J., Li, L., Xia, X., Leng, C., and Huang, G.: Insights into summertime haze pollution events over Shanghai based on online water-soluble ionic composition of aerosols, Atmospheric Environment, 45, 5131-5137, 2011.
Dunford, H. B.: Oxidations of iron (II)/(III) by hydrogen peroxide: from aquo to enzyme, Coordination Chemistry Reviews, 233, 311-318, 2002.
Ervens, B., Gligorovski, S., and Herrmann, H.: Temperature-dependent rate constants for hydroxyl radical reactions with organic compounds in aqueous solutions, Phys Chem Chem Phys, 5, 1811-1824, Doi 10.1039/B300072a, 2003.
Ervens, B., Feingold, G., Frost, G. J., and Kreidenweis, S. M.: A modeling study of aqueous production of dicarboxylic acids: 1. Chemical pathways and speciated organic mass production, Journal of Geophysical Research-Atmospheres, 109, D15205, 10.1029/2003jd004387, 2004.
Ervens, B., and Volkamer, R.: Glyoxal processing by aerosol multiphase chemistry: towards a kinetic modeling framework of secondary organic aerosol formation in aqueous particles, Atmospheric Chemistry and Physics, 10, 8219-8244, DOI

10.5194/acp-10-8219-2010, 2010.
Ervens, B., Turpin, B. J., and Weber, R. J.: Secondary organic aerosol formation in cloud droplets and aqueous particles (aqSOA): a review of laboratory, field and model studies, Atmospheric Chemistry and Physics, 11, 11069-11102, 10.5194/acp-11-11069-2011, 2011.
Ervens, B., Sorooshian, A., Lim, Y. B., and Turpin, B. J.: Key parameters controlling OH-initiated formation of secondary organic aerosol in the aqueous phase (aqSOA), Journal of Geophysical Research-Atmospheres, 119, 3997-4016, 10.1002/2013JD021021, 2014.
Ervens, B.: Modeling the Processing of Aerosol and Trace Gases in Clouds and Fogs, Chem Rev, 115, 4157-4198, 10.1021/cr5005887, 2015.
Fenton, H.: LXXIII.—Oxidation of tartaric acid in presence of iron, Journal of the Chemical Society, Transactions, 65, 899-910, 1894.
Fountoukis, C., and Nenes, A.: ISORROPIA II: a computationally efficient thermodynamic equilibrium model for K+–Ca 2+–Mg 2+–NH 4+–Na+–SO 4 2−–NO 3−–Cl−–H 2 O aerosols, Atmospheric Chemistry and Physics, 7, 4639-4659, 2007.
Galloway, M. M., Chhabra, P. S., Chan, A. W. H., Surratt, J. D., Flagan, R. C., Seinfeld, J. H., and Keutsch, F. N.: Glyoxal uptake on ammonium sulphate seed aerosol: reaction products and reversibility of uptake under dark and irradiated conditions, Atmospheric Chemistry and Physics, 9, 3331-3345, 10.5194/acp-9-3331-2009, 2009.
Gligorovski, S., Strekowski, R., Barbati, S., and Vione, D.: Environmental Implications of Hydroxyl Radicals (•OH), Chem Rev, 115, 13051-13092, 10.1021/cr500310b, 2015.
Goldstein, A. H., and Galbally, I. E.: Known and unexplored organic constituents in the earth's atmosphere, Environmental Science & Technology, 41, 1514-1521, Doi 10.1021/Es072476p, 2007.
Hallquist, M., Wenger, J. C., Baltensperger, U., Rudich, Y., Simpson, D., Claeys, M., Dommen, J., Donahue, N. M., George, C., Goldstein, A. H., Hamilton, J. F., Herrmann, H., Hoffmann, T., Iinuma, Y., Jang, M., Jenkin, M. E., Jimenez, J. L., Kiendler-Scharr, A., Maenhaut, W., McFiggans, G., Mentel, T. F., Monod, A., Prévôt, A. S. H., Seinfeld, J. H., Surratt, J. D., Szmigielski, R., and Wildt, J.: The formation, properties and impact of secondary organic aerosol: current and emerging issues, Atmospheric Chemistry and Physics, 9, 5155-5236, 10.5194/acp-9-5155-2009, 2009.
Hanson, D. R., Burkholder, J. B., Howard, C. J., and Ravishankara, A.: Measurement of hydroxyl and hydroperoxy radical uptake coefficients on water and sulfuric acid surfaces, The Journal of Physical Chemistry, 96, 4979-4985, 1992.
Hatch, L. E., Creamean, J. M., Ault, A. P., Surratt, J. D., Chan, M. N., Seinfeld, J. H., Edgerton, E. S., Su, Y., and Prather, K. A.: Measurements of isoprene-derived organosulfates in ambient aerosols by aerosol time-of-flight mass spectrometry-Part 1: Single particle atmospheric observations in Atlanta, Environmental science & technology, 45, 5105-5111, 2011.

Herrmann, H.: Kinetics of aqueous phase reactions relevant for atmospheric chemistry, Chem Rev, 103, 4691-4716, Doi 10.1021/Cr020658q, 2003.
Herrmann, H., Tilgner, A., Barzaghi, P., Majdik, Z., Gligorovski, S., Poulain, L., and Monod, A.: Towards a more detailed description of tropospheric aqueous phase organic chemistry: CAPRAM 3.0, Atmospheric Environment, 39, 4351-4363, 10.1016/j.atmosenv.2005.02.016, 2005.
Herrmann, H., Schaefer, T., Tilgner, A., Styler, S. A., Weller, C., Teich, M., and Otto, T.: Tropospheric Aqueous-Phase Chemistry: Kinetics, Mechanisms, and Its Coupling to a Changing Gas Phase, Chem Rev, 115, 4259-4334, 10.1021/cr500447k, 2015.
Ho, K. F., Cao, J. J., Lee, S. C., Kawamura, K., Zhang, R. J., Chow, J. C., and Watson, J. G.: Dicarboxylic acids, ketocarboxylic acids, and dicarbonyls in the urban atmosphere of China, Journal of Geophysical Research-Atmospheres, 112, D22S27, 10.1029/2006jd008011, 2007.
Ho, K. F., Lee, S. C., Ho, S. S. H., Kawamura, K., Tachibana, E., Cheng, Y., and Zhu, T.: Dicarboxylic acids, ketocarboxylic acids, alpha-dicarbonyls, fatty acids, and benzoic acid in urban aerosols collected during the 2006 Campaign of Air Quality Research in Beijing (CAREBeijing-2006), Journal of Geophysical Research-Atmospheres, 115, D19312, 10.1029/2009jd013304, 2010.
Ho, K. F., Ho, S. S. H., Lee, S. C., Kawamura, K., Zou, S. C., Cao, J. J., and Xu, H. M.: Summer and winter variations of dicarboxylic acids, fatty acids and benzoic acid in PM(2.5) in Pearl Delta River Region, China, Atmospheric Chemistry and Physics, 11, 2197-2208, 10.5194/acp-11-2197-2011, 2011.
Huang, X.-F., and Yu, J. Z.: Is vehicle exhaust a significant primary source of oxalic acid in ambient aerosols?, Geophysical Research Letters, 34, L02808, 10.1029/2006gl028457, 2007.
Jimenez, J. L., Canagaratna, M. R., Donahue, N. M., Prevot, A. S. H., Zhang, Q., Kroll, J. H., DeCarlo, P. F., Allan, J. D., Coe, H., Ng, N. L., Aiken, A. C., Docherty, K. S., Ulbrich, I. M., Grieshop, A. P., Robinson, A. L., Duplissy, J., Smith, J. D., Wilson, K. R., Lanz, V. A., Hueglin, C., Sun, Y. L., Tian, J., Laaksonen, A., Raatikainen, T., Rautiainen, J., Vaattovaara, P., Ehn, M., Kulmala, M., Tomlinson, J. M., Collins, D. R., Cubison, M. J., Dunlea, E. J., Huffman, J. A., Onasch, T. B., Alfarra, M. R., Williams, P. I., Bower, K., Kondo, Y., Schneider, J., Drewnick, F., Borrmann, S., Weimer, S., Demerjian, K., Salcedo, D., Cottrell, L., Griffin, R., Takami, A., Miyoshi, T., Hatakeyama, S., Shimono, A., Sun, J. Y., Zhang, Y. M., Dzepina, K., Kimmel, J. R., Sueper, D., Jayne, J. T., Herndon, S. C., Trimborn, A. M., Williams, L. R., Wood, E. C., Middlebrook, A. M., Kolb, C. E., Baltensperger, U., and Worsnop, D. R.: Evolution of Organic Aerosols in the Atmosphere, Science, 326, 1525-1529, 10.1126/science.1180353, 2009.
Kawamura, K., and Ikushima, K.: seasonal-changes in the distribution of dicarboxylic-acids in the urban atmosphere, Environmental Science & Technology, 27, 2227-2235, 10.1021/es00047a033, 1993.
Kawamura, K., Kobayashi, M., Tsubonuma, N., Mochida, M., Watanabe, T., and Lee,

M.: Organic and inorganic compositions of marine aerosols from East Asia: Seasonal variations of water-soluble dicarboxylic acids, major ions, total carbon and nitrogen, and stable C and N isotopic composition, Geochemical Investigations in Earth and Space Science: A Tribute to Issac R. Kaplan, 9, edited by: Hill, R. J. L. J. A. Z. B. M. J. C. G., and Eganhouse, R. G. M. P. K., 243-265 pp., 2004.

Kawamura, K., and Yasui, O.: Diurnal changes in the distribution of dicarboxylic acids, ketocarboxylic acids and dicarbonyls in the urban Tokyo atmosphere, Atmospheric Environment, 39, 1945-1960, 10.1016/j.atmosenv.2004.12.014, 2005.

Kawamura, K., Kasukabe, H., and Barrie, L. A.: Secondary formation of water-soluble organic acids and alpha-dicarbonyls and their contributions to total carbon and water-soluble organic carbon: Photochemical aging of organic aerosols in the Arctic spring, Journal of Geophysical Research-Atmospheres, 115, D21306, 10.1029/2010jd014299, 2010.

Kawamura, K., Tachibana, E., Okuzawa, K., Aggarwal, S. G., Kanaya, Y., and Wang, Z. F.: High abundances of water-soluble dicarboxylic acids, ketocarboxylic acids and alpha-dicarbonyls in the mountaintop aerosols over the North China Plain during wheat burning season, Atmospheric Chemistry and Physics, 13, 8285-8302, 10.5194/acp-13-8285-2013, 2013.

Khezri, B., Mo, H., Yan, Z., Chong, S.-L., Heng, A. K., and Webster, R. D.: Simultaneous online monitoring of inorganic compounds in aerosols and gases in an industrialized area, Atmospheric Environment, 80, 352-360, 2013.

Kremer, M. L.: The Fenton reaction. Dependence of the rate on pH, Journal of Physical Chemistry A, 107, 1734-1741, 10.1021/jp020654p, 2003.

Kundu, S., Kawamura, K., Andreae, T. W., Hoffer, A., and Andreae, M. O.: Molecular distributions of dicarboxylic acids, ketocarboxylic acids and alpha-dicarbonyls in biomass burning aerosols: implications for photochemical production and degradation in smoke layers, Atmospheric Chemistry and Physics, 10, 2209-2225, 10.5194/acp-10-2209-2010, 2010.

Li, L., Huang, Z. X., Dong, J. G., Li, M., Gao, W., Nian, H. Q., Fu, Z., Zhang, G. H., Bi, X. H., Cheng, P., and Zhou, Z.: Real time bipolar time-of-flight mass spectrometer for analyzing single aerosol particles, Int J Mass Spectrom, 303, 118-124, 10.1016/j.ijms.2011.01.017, 2011.

Li, L., Li, M., Huang, Z., Gao, W., Nian, H., Fu, Z., Gao, J., Chai, F., and Zhou, Z.: Ambient particle characterization by single particle aerosol mass spectrometry in an urban area of Beijing, Atmospheric Environment, 94, 323-331, 2014.

Lim, Y. B., Tan, Y., Perri, M. J., Seitzinger, S. P., and Turpin, B. J.: Aqueous chemistry and its role in secondary organic aerosol (SOA) formation, Atmospheric Chemistry and Physics, 10, 10521-10539, 10.5194/acp-10-10521-2010, 2010.

Ma, Q. X., He, H., and Liu, C.: Hygroscopic properties of oxalic acid and atmospherically relevant oxalates, Atmospheric Environment, 69, 281-288, 10.1016/j.atmosenv.2012.12.011, 2013.

Ma, S. X., Ren, K., Liu, X. W., Chen, L. G., Li, M., Li, X. Y., Yang, J., Huang, B.,

729 Zheng, M., and Xu, Z. C.: Production of hydroxyl radicals from Fe-containing
730 fine particles in Guangzhou, China, Atmospheric Environment, 123, 72-78,
731 10.1016/j.atmosenv.2015.10.057, 2015.
732 McNeill, V. F.: Aqueous organic chemistry in the atmosphere: Sources and chemical
733 processing of organic aerosols, Environmental science & technology, 49,
734 1237-1244, 2015.
735 Meng, J. J., Wang, G. H., Li, J. J., Cheng, C. L., and Cao, J. J.: Atmospheric oxalic
736 acid and related secondary organic aerosols in Qinghai Lake, a continental
737 background site in Tibet Plateau, Atmospheric Environment, 79, 582-589,
738 10.1016/j.atmosenv.2013.07.024, 2013.
739 Meng, J. J., Wang, G. H., Li, J. J., Cheng, C. L., Ren, Y. Q., Huang, Y., Cheng, Y. T.,
740 Cao, J. J., and Zhang, T.: Seasonal characteristics of oxalic acid and related SOA
741 in the free troposphere of Mt. Hua, central China: Implications for sources and
742 formation mechanisms, Science Of The Total Environment, 493, 1088-1097,
743 10.1016/j.scitotenv.2014.04.086, 2014.
744 Miyazaki, Y., Aggarwal, S. G., Singh, K., Gupta, P. K., and Kawamura, K.:
745 Dicarboxylic acids and water-soluble organic carbon in aerosols in New Delhi,
746 India, in winter: Characteristics and formation processes, Journal of Geophysical
747 Research-Atmospheres, 114, D19206, 10.1029/2009jd011790, 2009.
748 Moffet, R. C., de Foy, B., Molina, L. T., Molina, M. J., and Prather, K. A.:
749 Measurement of ambient aerosols in northern Mexico City by single particle
750 mass spectrometry, Atmospheric Chemistry and Physics, 8, 4499-4516,
751 10.5194/acp-8-4499-2008, 2008.
752 Myriokefalitakis, S., Tsigaridis, K., Mihalopoulos, N., Sciare, J., Nenes, A.,
753 Kawamura, K., Segers, A., and Kanakidou, M.: In-cloud oxalate formation in the
754 global troposphere: a 3-D modeling study, Atmospheric Chemistry and Physics,
755 11, 5761-5782, 10.5194/acp-11-5761-2011, 2011.
756 Nenes, A., Pandis, S. N., and Pilinis, C.: ISORROPIA: A new thermodynamic
757 equilibrium model for multiphase multicomponent inorganic aerosols, Aquatic
758 geochemistry, 4, 123-152, 1998.
759 Nenes, A., Pandis, S. N., and Pilinis, C.: Continued development and testing of a new
760 thermodynamic aerosol module for urban and regional air quality models,
761 Atmospheric Environment, 33, 1553-1560, 1999.
762 Noble, C. A., and Prather, K. A.: Real-time measurement of correlated size and
763 composition profiles of individual atmospheric aerosol particles, Environmental
764 science & technology, 30, 2667-2680, 1996.
765 Novakov, T., and Penner, J. E.: Large Contribution of Organic Aerosols to
766 Cloud-Condensation-Nuclei Concentrations, Nature, 365, 823-826, Doi
767 10.1038/365823a0, 1993.
768 Pavuluri, C. M., Kawamura, K., and Swaminathan, T.: Water-soluble organic carbon,
769 dicarboxylic acids, ketoacids, and alpha-dicarbonyls in the tropical Indian
770 aerosols, Journal of Geophysical Research-Atmospheres, 115, D11302,
771 10.1029/2009JD012661, 2010.
772 Poschl, U., and Shiraiwa, M.: Multiphase Chemistry at the Atmosphere-Biosphere

Interface Influencing Climate and Public Health in the Anthropocene, Chem Rev, 115, 4440-4475, 10.1021/cr500487s, 2015.

Prather, K. A., Nordmeyer, T., and Salt, K.: Real-time characterization of individual aerosol particles using time-of-flight mass spectrometry, Anal. Chem., 66, 1403-1407, 1994.

Pratt, K. A., Hatch, L. E., and Prather, K. A.: Seasonal Volatility Dependence of Ambient Particle Phase Amines, Environmental Science & Technology, 43, 5276-5281, 10.1021/es803189n, 2009.

Prenni, A. J., De Mott, P. J., and Kreidenweis, S. M.: Water uptake of internally mixed particles containing ammonium sulfate and dicarboxylic acids, Atmospheric Environment, 37, 4243-4251, 10.1016/s1352-2310(03)00559-4, 2003.

Silva, P. J., and Prather, K. A.: Interpretation of mass spectra from organic compounds in aerosol time-of-flight mass spectrometry, Analytical Chemistry, 72, 3553-3562, 2000.

Sorooshian, A., Varutbangkul, V., Brechtel, F. J., Ervens, B., Feingold, G., Bahreini, R., Murphy, S. M., Holloway, J. S., Atlas, E. L., Buzorius, G., Jonsson, H., Flagan, R. C., and Seinfeld, J. H.: Oxalic acid in clear and cloudy atmospheres: Analysis of data from International Consortium for Atmospheric Research on Transport and Transformation 2004, Journal of Geophysical Research-Atmospheres, 111, 10.1029/2005jd006880, 2006.

Sorooshian, A., Lu, M.-L., Brechtel, F. J., Jonsson, H., Feingold, G., Flagan, R. C., and Seinfeld, J. H.: On the source of organic acid aerosol layers above clouds, Environmental Science & Technology, 41, 4647-4654, 10.1021/es0630442, 2007a.

Sorooshian, A., Ng, N. L., Chan, A. W. H., Feingold, G., Flagan, R. C., and Seinfeld, J. H.: Particulate organic acids and overall water-soluble aerosol composition measurements from the 2006 Gulf of Mexico Atmospheric Composition and Climate Study (GoMACCS), Journal of Geophysical Research-Atmospheres, 112, 10.1029/2007jd008537, 2007b.

Sorooshian, A., Wang, Z., Coggon, M. M., Jonsson, H. H., and Ervens, B.: Observations of Sharp Oxalate Reductions in Stratocumulus Clouds at Variable Altitudes: Organic Acid and Metal Measurements During the 2011 E-PEACE Campaign, Environmental Science & Technology, 47, 7747-7756, 10.1021/es4012383, 2013.

Stone, E. A., Hedman, C. J., Zhou, J. B., Mieritz, M., and Schauer, J. J.: Insights into the nature of secondary organic aerosol in Mexico City during the MILAGRO experiment 2006, Atmospheric Environment, 44, 312-319, 10.1016/j.atmosenv.2009.10.036, 2010.

Sullivan, R. C., and Prather, K. A.: Investigations of the diurnal cycle and mixing state of oxalic acid in individual particles in Asian aerosol outflow, Environmental Science Technology, 41, 8062-8069, 2007a.

Sullivan, R. C., and Prather, K. A.: Investigations of the diurnal cycle and mixing state of oxalic acid in individual particles in Asian aerosol outflow, Environmental Science & Technology, 41, 8062-8069, 10.1021/es071134g, 2007b.

Surratt, J. D., Kroll, J. H., Kleindienst, T. E., Edney, E. O., Claeys, M., Sorooshian, A., Ng, N. L., Offenberg, J. H., Lewandowski, M., Jaoui, M., Flagan, R. C., and Seinfeld, J. H.: Evidence for organosulfates in secondary organic aerosol, Environmental Science & Technology, 41, 517-527, 10.1021/Es062081q, 2007.

Surratt, J. D., Gomez-Gonzalez, Y., Chan, A. W. H., Vermeylen, R., Shahgholi, M., Kleindienst, T. E., Edney, E. O., Offenberg, J. H., Lewandowski, M., Jaoui, M., Maenhaut, W., Claeys, M., Flagan, R. C., and Seinfeld, J. H.: Organosulfate formation in biogenic secondary organic aerosol, Journal of Physical Chemistry A, 112, 8345-8378, Doi 10.1021/Jp802310p, 2008.

Tan, Y., Perri, M. J., Seitzinger, S. P., and Turpin, B. J.: Effects of Precursor Concentration and Acidic Sulfate in Aqueous Glyoxal-OH Radical Oxidation and Implications for Secondary Organic Aerosol, Environmental Science & Technology, 43, 8105-8112, 10.1021/Es901742f, 2009.

ten Brink, H., Otjes, R., Jongejan, P., and Slanina, S.: An instrument for semi-continuous monitoring of the size-distribution of nitrate, ammonium, sulphate and chloride in aerosol, Atmospheric Environment, 41, 2768-2779, 2007.

Tong, H. J., Arangio, A. M., Lakey, P. S. J., Berkemeier, T., Liu, F. B., Kampf, C. J., Brune, W. H., Poschl, U., and Shiraiwa, M.: Hydroxyl radicals from secondary organic aerosol decomposition in water, Atmospheric Chemistry and Physics, 16, 1761-1771, 10.5194/acp-16-1761-2016, 2016.

van Pinxteren, D., Neususs, C., and Herrmann, H.: On the abundance and source contributions of dicarboxylic acids in size-resolved aerosol particles at continental sites in central Europe, Atmospheric Chemistry and Physics, 14, 3913-3928, 10.5194/acp-14-3913-2014, 2014.

Wang, G., Cheng, C., Meng, J., Huang, Y., Li, J., and Ren, Y.: Field observation on secondary organic aerosols during Asian dust storm periods: Formation mechanism of oxalic acid and related compounds on dust surface, Atmospheric Environment, 113, 169-176, 2015.

Wang, G., Zhang, R., Gomez, M. E., Yang, L., Levy Zamora, M., Hu, M., Lin, Y., Peng, J., Guo, S., Meng, J., Li, J., Cheng, C., Hu, T., Ren, Y., Wang, Y., Gao, J., Cao, J., An, Z., Zhou, W., Li, G., Wang, J., Tian, P., Marrero-Ortiz, W., Secrest, J., Du, Z., Zheng, J., Shang, D., Zeng, L., Shao, M., Wang, W., Huang, Y., Wang, Y., Zhu, Y., Li, Y., Hu, J., Pan, B., Cai, L., Cheng, Y., Ji, Y., Zhang, F., Rosenfeld, D., Liss, P. S., Duce, R. A., Kolb, C. E., and Molina, M. J.: Persistent sulfate formation from London Fog to Chinese haze, Proceedings of the National Academy of Sciences, 113, 13630-13635, 10.1073/pnas.1616540113, 2016.

Wang, G. H., Kawamura, K., Cheng, C. L., Li, J. J., Cao, J. J., Zhang, R. J., Zhang, T., Liu, S. X., and Zhao, Z. Z.: Molecular Distribution and Stable Carbon Isotopic Composition of Dicarboxylic Acids, Ketocarboxylic Acids, and alpha-Dicarbonyls in Size-Resolved Atmospheric Particles From Xi'an City, China, Environmental Science & Technology, 46, 4783-4791, 10.1021/es204322c, 2012.

Wang, J. Y., Wang, G. H., Gao, J., Wang, H., Ren, Y. Q., Li, J. J., Wu, C., Zhang, L.,

Wang, S. L., and Chai, F. H.: Concentrations and stable carbon isotope compositions of oxalic acid and related SOA in Beijing before, during and after the 2014 APEC, Atmospheric Chemistry and Physics 17, 981-992, 2017.

Weller, C., Tilgner, A., Brauer, P., and Herrmann, H.: Modeling the Impact of Iron-Carboxylate Photochemistry on Radical Budget and Carboxylate Degradation in Cloud Droplets and Particles, Environmental Science & Technology, 48, 5652-5659, 10.1021/es4056643, 2014.

Wonaschuetz, A., Sorooshian, A., Ervens, B., Chuang, P. Y., Feingold, G., Murphy, S. M., de Gouw, J., Warneke, C., and Jonsson, H. H.: Aerosol and gas re-distribution by shallow cumulus clouds: An investigation using airborne measurements, Journal of Geophysical Research-Atmospheres, 117, 10.1029/2012jd018089, 2012.

Xue, J., Lau, A. K. H., and Yu, J. Z.: A study of acidity on PM2.5 in Hong Kong using online ionic chemical composition measurements, Atmospheric Environment, 45, 7081-7088, 10.1016/j.atmosenv.2011.09.040, 2011.

Yang, F., Chen, H., Wang, X., Yang, X., Du, J., and Chen, J.: Single particle mass spectrometry of oxalic acid in ambient aerosols in Shanghai: Mixing state and formation mechanism, Atmospheric Environment, 43, 3876-3882, 2009.

Yao, X. H., Fang, M., and Chan, C. K.: Size distributions and formation of dicarboxylic acids in atmospheric particles, Atmospheric Environment, 36, 2099-2107, 2002.

Yao, X. H., Lau, A. P. S., Fang, M., Chan, C. K., and Hu, M.: Size distributions and formation of ionic species in atmospheric particulate pollutants in Beijing, China: 2 - dicarboxylic acids, Atmospheric Environment, 37, 3001-3007, 10.1016/s1352-2310(03)00256-5, 2003.

Yu, J. Z., Huang, X. F., Xu, J. H., and Hu, M.: When aerosol sulfate goes up, so does oxalate: Implication for the formation mechanisms of oxalate, Environmental Science & Technology, 39, 128-133, 10.1021/Es049559f, 2005.

Yu, L., Smith, J., Laskin, A., Anastasio, C., Laskin, J., and Zhang, Q.: Chemical characterization of SOA formed from aqueous-phase reactions of phenols with the triplet excited state of carbonyl and hydroxyl radical, Atmospheric Chemistry and Physics, 14, 13801-13816, 10.5194/acp-14-13801-2014, 2014.

Zauscher, M. D., Wang, Y., Moore, M. J. K., Gaston, C. J., and Prather, K. A.: Air Quality Impact and Physicochemical Aging of Biomass Burning Aerosols during the 2007 San Diego Wildfires, Environmental Science & Technology, 47, 7633-7643, 10.1021/es4004137, 2013.

Zhang, G., Bi, X., Li, L., Chan, L. Y., Li, M., Wang, X., Sheng, G., Fu, J., and Zhou, Z.: Mixing state of individual submicron carbon-containing particles during spring and fall seasons in urban Guangzhou, China: a case study, Atmospheric Chemistry and Physics, 13, 4723-4735, 2013.

Zhang, G., Bi, X., He, J., Chen, D., Chan, L. Y., Xie, G., Wang, X., Sheng, G., Fu, J., and Zhou, Z.: Variation of secondary coatings associated with elemental carbon by single particle analysis, Atmospheric Environment, 92, 162-170, 2014.

Zhang, R., Wang, G., Guo, S., Zamora, M. L., Ying, Q., Lin, Y., Wang, W., Hu, M.,

and Wang, Y.: Formation of urban fine particulate matter, Chem Rev, 115, 3803-3855, 2015.

Zhou, Y., Huang, X. H., Bian, Q., Griffith, S. M., Louie, P. K., and Yu, J. Z.: Sources and atmospheric processes impacting oxalate at a suburban coastal site in Hong Kong: Insights inferred from 1 year hourly measurements, Journal of Geophysical Research: Atmospheres, 120, 9772-9788, 2015.

# Tables and Figures

**Table list:**

Table 1. Summary of major groups of oxalic acid-containing particles in summer and winter in PRD, China.

Table 2. The abundance of major particle types in total oxalic acid-containing particles during the episode in winter (2/8/2015).

**Figure caption:**

Figure 1. Temporal variations of total detected particles and oxalic acid containing particles during whole sampling periods in Heshan, China: (a) hourly variations of $PM_{2.5}$ mass concentration, total detected particle counts, oxalic acid containing particles, ratio of oxalic acid-containing/total particles and major types of oxalic acid containing particles; (b) variation patterns of relative abundance of major types of oxalic acid containing particles.

Figure 2. The averaged positive and negative ion mass spectra of oxalic acid containing particles is investigated in summer and winter: (a) summer positive, (b) summer negative, (c) winter positive, (d) winter negative. The color bars represent each peak area corresponding to specific fraction in individual particles.

Figure 3. (a) Mixing state of oxalic acid with sulfate, nitrate and ammonium in oxalic acid-containing particles; (b) Linear correlation between $NH_4^+$-containing oxalic acid particles and the total oxalic acid particles in summer; (c) Linear correlation between $NH_4^+$-containing oxalic acid particles and the total oxalic acid particles in winter. Abbreviations: $C_2$-$NH_4^+$ represents the $NH_4^+$-containing oxalic acid particles, and same expressions for $C_2$-$SO_4^{2-}$ and $C_2$-$NO_3^-$.

Figure 4. Unscaled size-resolved number distributions of major types of oxalic acid particles in summer and winter.

Figure 5. Temporal variations of $O_3$ concentrations, oxalic acid particles, malonic acid particles and heavy metal type of oxalic acid particles during the entire sampling period in Heshan, China.

Figure 6. The averaged digitized positive and negative ion mass spectra of heavy metal type of oxalic acid-containing particles in summer.

Figure 7. The diurnal variations of $O_3$ concentration, oxalic acid particles, HM group particles and in-situ pH ($pH_{is}$) from July 28 to August 1 in 2014.

Figure 8. The temporal variations of peak area of nitrate, sulfate and oxalic acid, and the relative acidity ratio ($R_{ra}$) in carbonaceous type oxalic acid particles in winter.

Figure 9. The comprehensive study of oxalic acid particles increase on Feb 8, 2015: (a) The digitized positive and negative ion mass spectrum of oxalic acid particles during the episode; (b) Linear regression between total oxalic acid particles and organosulfate-containing oxalic acid particles (m/z -155).

1010

Table 1. Summary of major groups of oxalic acid-containing particles in summer and winter in PRD, China.

| | Summer(7/18-8/1, 2014) | | Winter(1/27-2/8, 2015) | |
|---|---|---|---|---|
| Particle type | Count | Percentage, % | Count | Percentage, % |
| EC | 1473 | 11.2 | 3161 | 15.4 |
| ECOC | 41 | 0.3 | 2233 | 10.9 |
| OC | 473 | 3.6 | 1922 | 9.4 |
| BB | 1702 | 13.0 | 4953 | 24.2 |
| HM | 4104 | 31.3 | 3124 | 15.2 |
| Sec | 2511 | 19.2 | 2192 | 10.7 |
| NaK | 303 | 2.3 | 17 | 0.1 |
| Dust | 1139 | 8.7 | 1888 | 9.2 |

Abbreviations of major particle types: elemental carbon (EC), elemental and organic carbon (ECOC), organic carbon (OC), biomass burning (BB), heavy metal (HM), secondary (Sec), sodium and potassium (NaK) and dust (Dust).

1011
1012
1013
1014
1015

Table 2. The abundance of major particle types in total oxalic acid-containing particles during the episode in winter (2/8/2015).

| | EC | ECOC | OC | BB | Sec | HM | Dust | other |
|---|---|---|---|---|---|---|---|---|
| Count | 1250 | 604 | 326 | 1320 | 856 | 377 | 814 | 132 |
| Percentage, % | 22.0 | 10.6 | 5.7 | 23.2 | 15.1 | 6.6 | 14.3 | 2.3 |

1016
1017
1018
1019
1020
1021
1022
1023
1024
1025
1026
1027
1028

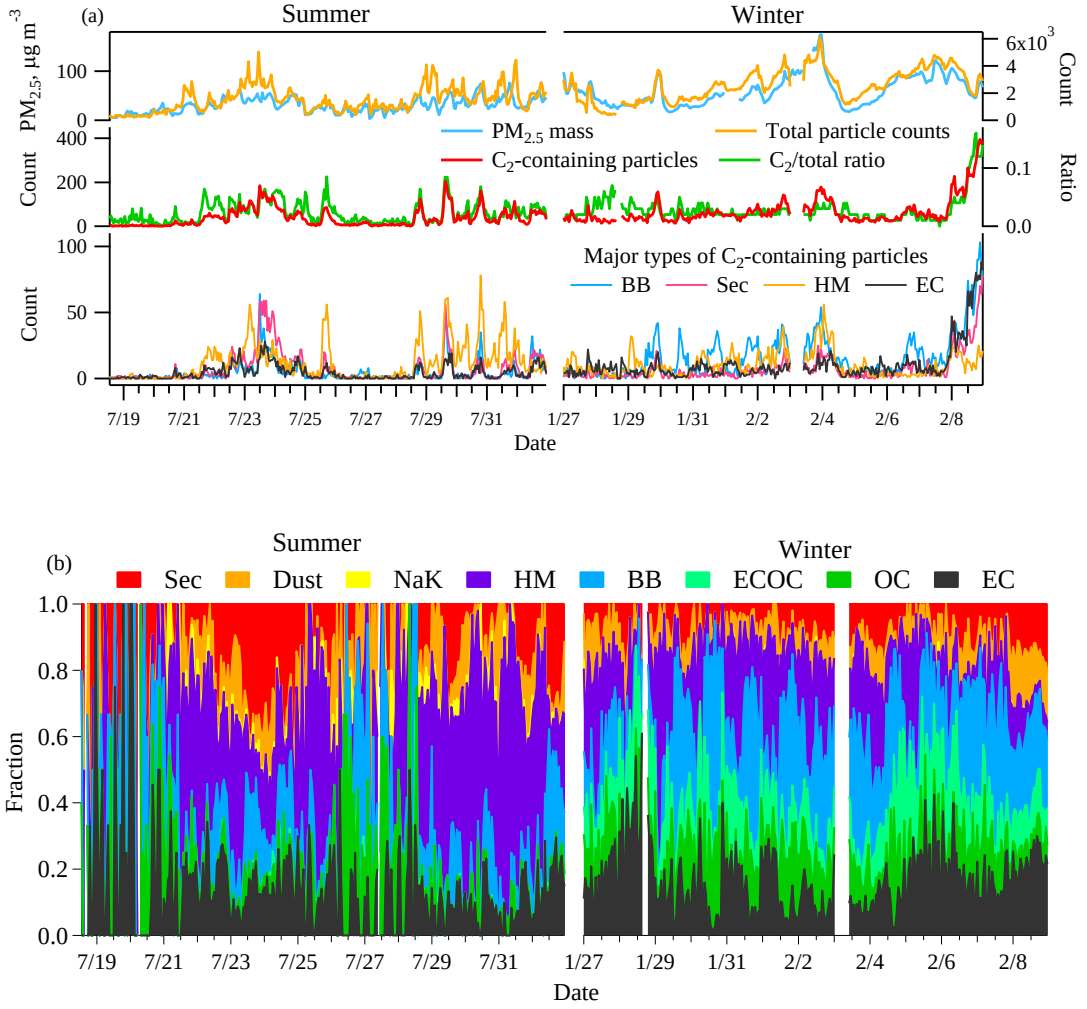


Figure 1. Temporal variations of total detected particles and oxalic acid containing particles during whole sampling periods in Heshan, China: (a) hourly variations of $PM_{2.5}$ mass concentration, total detected particle counts, oxalic acid containing particles, ratio of oxalic acid-containing/total particles and major types of oxalic acid containing particles; (b) variation patterns of relative abundance of major types of oxalic acid containing particles. Abbreviations of major particle types: elemental carbon (EC), organic carbon (OC), elemental and organic carbon (ECOC), biomass burning (BB), heavy metal (HM), secondary (Sec), sodium and potassium (NaK) and dust.

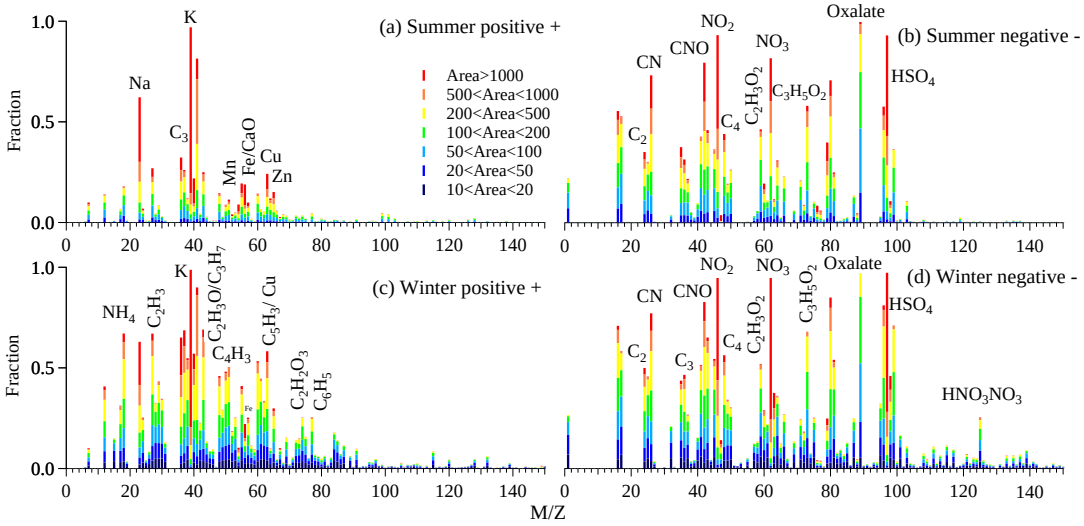


Figure 2. The averaged positive and negative ion mass spectra of oxalic acid containing particles is investigated in summer and winter: (a) summer positive, (b) summer negative, (c) winter positive, (d) winter negative. The color bars represent each peak area corresponding to specific fraction in individual particles.

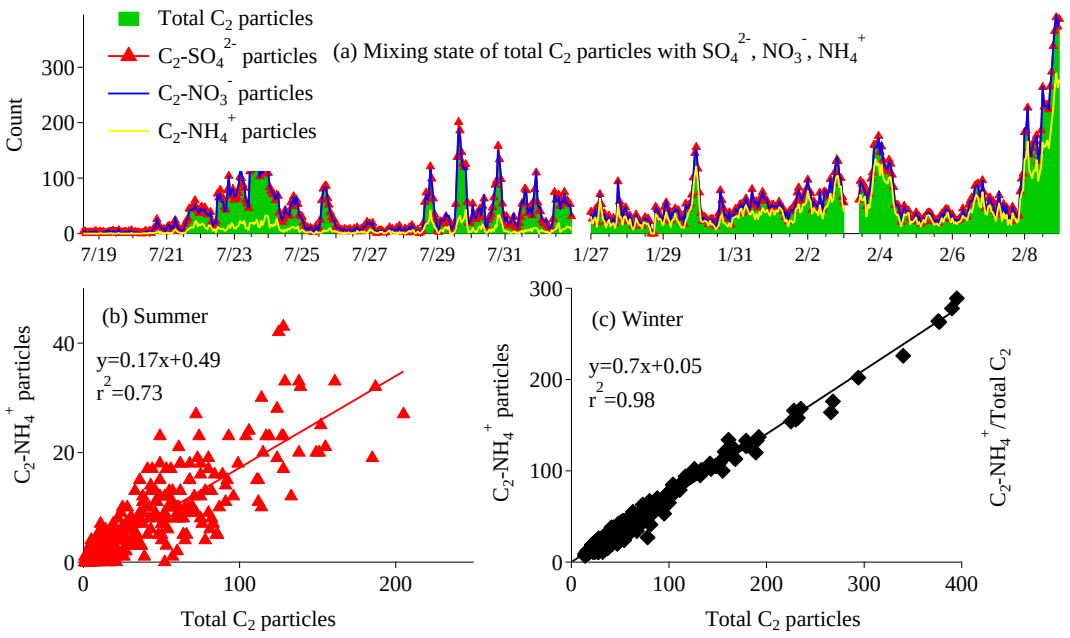


Figure 3. (a) Mixing state of oxalic acid with sulfate, nitrate and ammonium in oxalic acid-containing particles; (b) Linear correlation between $NH_4^+$-containing oxalic acid particles and the total oxalic acid particles in summer; (c) Linear correlation between $NH_4^+$-containing oxalic acid particles and the total oxalic acid particles in winter. Abbreviations: $C_2$-$NH_4^+$ represents the $NH_4^+$-containing oxalic acid particles, and same expressions for $C_2$-$SO_4^{2-}$ and $C_2$-$NO_3^-$.

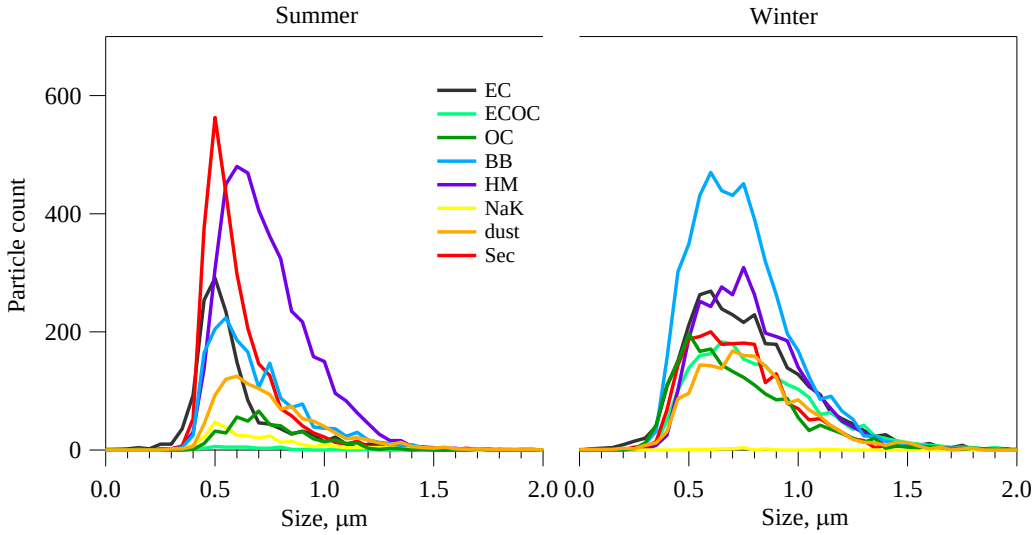


Figure 4. Unscaled size-resolved number distributions of major types of oxalic acid particles in summer and winter. Abbreviations of major particle types: elemental carbon (EC), organic carbon (OC), elemental and organic carbon (ECOC), biomass burning (BB), heavy metal (HM), secondary (Sec), sodium and potassium (NaK) and dust.

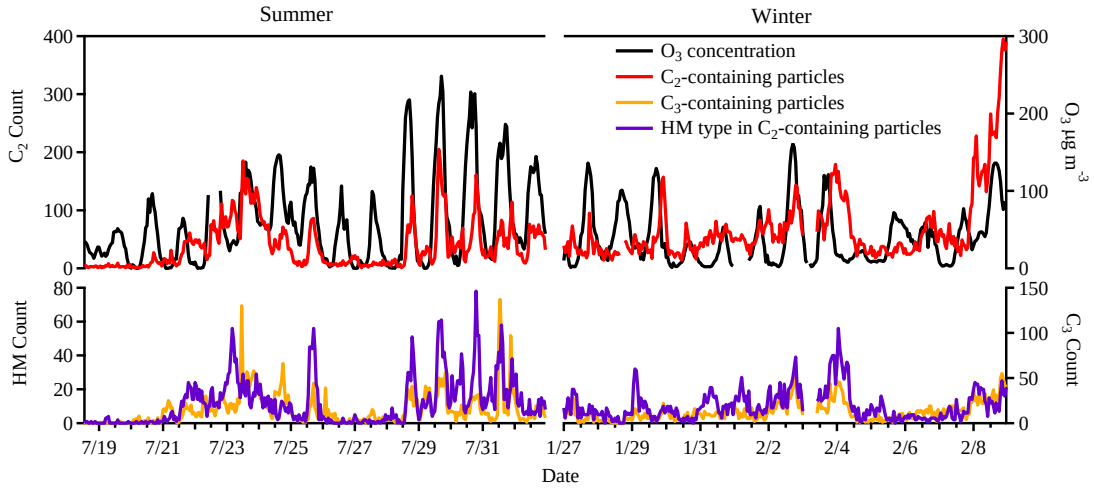


Figure 5. Temporal variations of $O_3$ concentrations, oxalic acid particles, malonic acid particles and heavy metal type of oxalic acid particles during the entire sampling period in Heshan, China.

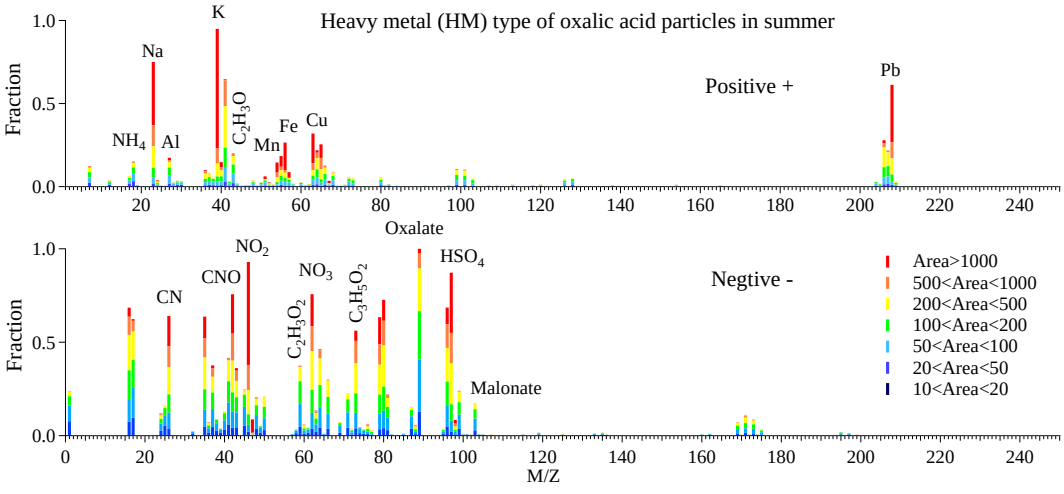


Figure 6. The averaged digitized positive and negative ion mass spectra of heavy metal type of oxalic acid-containing particles in summer.

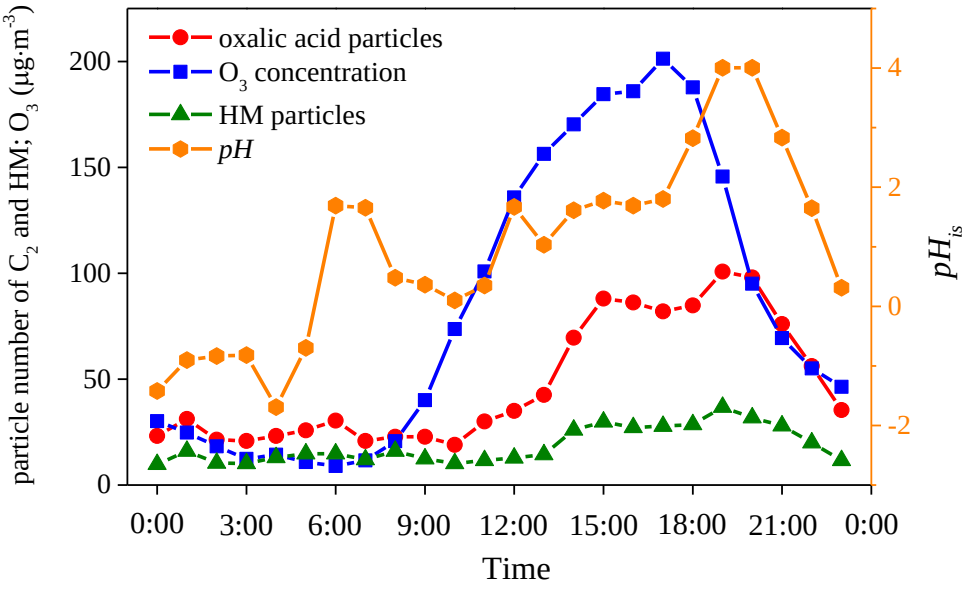


Figure 7. The diurnal variations of $O_3$ concentration, oxalic acid particles, HM group particles and in-situ pH ($pH_{is}$) from July 28 to August 1 in 2014.

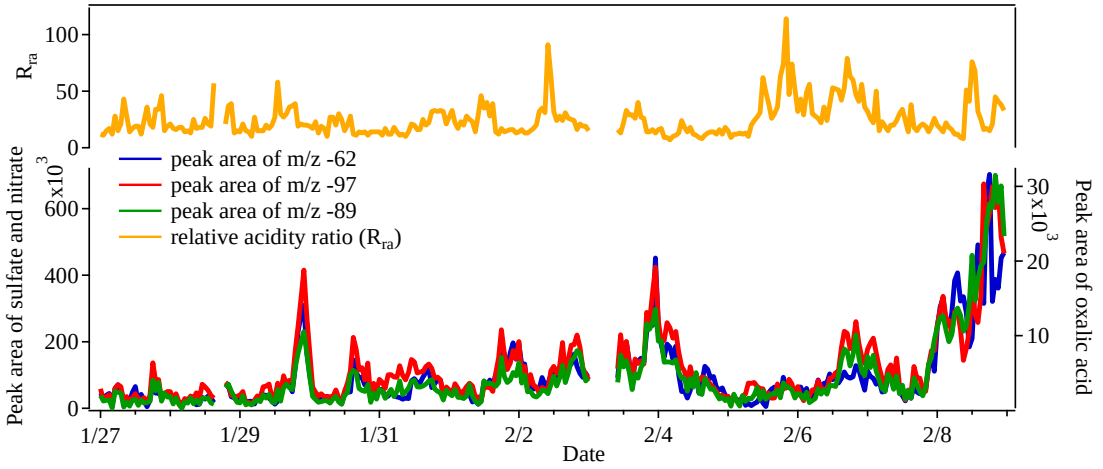


Figure 8. The temporal variations of peak area of nitrate, sulfate and oxalic acid, and the relative acidity ratio ($R_{ra}$) in carbonaceous type oxalic acid particles in winter.

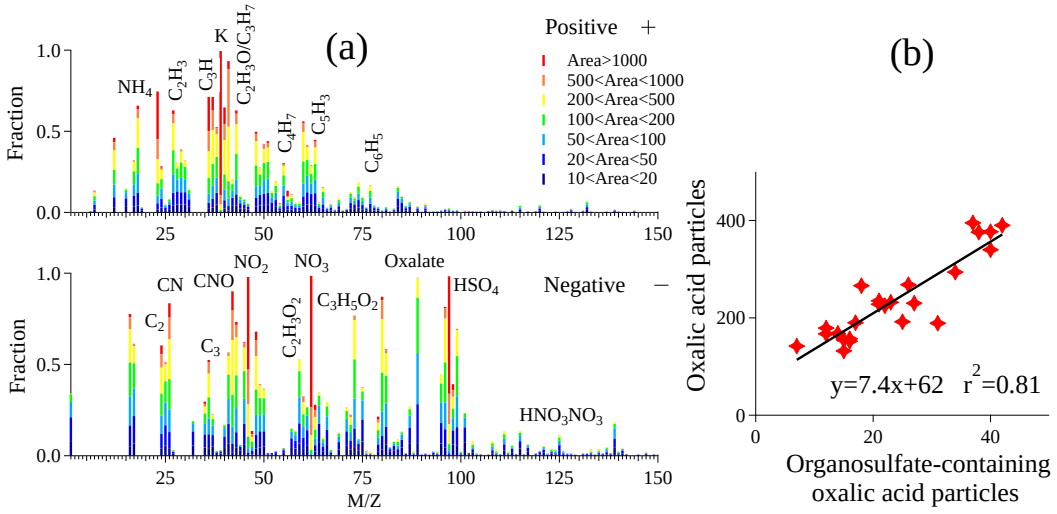


Figure 9. The comprehensive study of oxalic acid particles increase on Feb 8, 2015: (a) The digitized positive and negative ion mass spectrum of oxalic acid particles during the episode; (b) Linear regression between total oxalic acid particles and organosulfate-containing oxalic acid particles (m/z -155).